Full-Potential Integral Solution for Transonic Flows with and without Embedded Euler Domains

Osama A. Kandil* and Hong Hu†
Old Dominion University, Norfolk, Virginia

Two methods are presented to solve transonic airfoil flow problems. The first method is based on the integral equation solution of the full-potential equation in terms of the velocity field. A shock capturing-shock fitting scheme has been developed. In the shock-fitting part of the scheme, shock panels are introduced at the shock location. The shock panels are fitted by using the Rankine-Hugoniot relations. The second method is a coupling of the integral solution of the full-potential equation with the pseudotime integration of Euler equations, which are used in a small embedded region around the shock. This scheme is called the integral equation-embedded Euler scheme. The two methods are applied to NACA 0012 and 64A010A airfoils over a wide range of Mach numbers, and the results are in good agreement with the experimental data and other computational results. The schemes converge within a number of iterations that is one order of magnitude less than the finite-difference schemes.

Introduction

IN the finite-difference and finite-volume schemes, computation of transonic airfoil flow problems usually requires fine grids and large computational domains whose outer boundary usually extends 20–30 chord lengths away from the airfoil surface. The far-field boundary conditions are enforced on this boundary through a special process where a certain part of the boundary is treated as an inflow boundary, whereas the other part is treated as an outflow boundary. Conservative or nonconservative forms of the governing equations, which represent different levels of approximations, are solved by using relaxation schemes or pseudotime marching schemes to obtain the steady flow solution. Convergence is obtained within a number of iterations or time steps, which is typically of order of 1000. Using different levels of approximations, inviscid computational schemes have been developed. These schemes are based on the transonic small perturbation (TSP) equation,[1,2] full-potential (FP) equation,[3–5] and Euler equations.[5] Large computer memory is usually needed to handle the large number of grid points and the associated flow variables, and large CPU time is used to obtain converged solutions.

For flows with weak shocks, the potential equation that assumes irrotational isentropic flows can satisfactorily be used to solve for these flows, since the entropy increase across the shocks and vorticity production behind the shocks are small, and their effects are of high order. For strong shocks, the irrotational and isentropic flow assumptions are invalid, and one cannot use the potential flow equations across or behind the shocks. For these flows, one has to correct the potential equations in order to account for the entropy jump across the shock wave. Methods of this type have been developed by Hafez and Lovell,[7] Fuglsang and Williams,[8] and Whitlow et al.[9] Alternatively, one needs to use the computationally relatively expensive Euler equations.

The integral equation (IE) solution of the potential equation represents an alternative to the finite-difference and finite-element methods for solving transonic airfoil flow problems. The IE solution has several advantages in comparison with the finite-difference solution. With the IE formulation (IEF), the far-field boundary conditions are automatically satisfied, and only a small computational domain is needed around the source of disturbance. Moreover, the accuracy of the method depends on the evaluation of integrals rather than derivatives, and hence coarse grids can be used within the small computational domain. Because of the obvious advantages of the methods that are based on the IEF, it is highly desirable to develop these methods fully and extend them to treat transonic flows over a wide range of Mach numbers.

Computational schemes that are based on the IE formulation have recently been developed by several investigators. Piers and Sloof[10] and Tseng and Morino[11] have developed IE schemes for the TSP equation, while Kandil and Yates,[12] Oskam,[13] Erickson and Strande,[14] Sinclair,[15] and Kandil and Hu[16] have developed IE schemes for the FP equation. Since the potential equation cannot accurately treat flows with strong shocks, the IE schemes for the FP equation must be modified to accurately treat flows with strong shocks.

In this paper we present two methods to solve for the transonic airfoil flow problems that are based on the IE solution only or on the IE solution with small embedded Euler-domain solution. The latter method can efficiently treat flows with strong shocks. For the former method, a shock capturing-shock fitting (SCSF) scheme is developed, whereas for the latter method an integral equation-embedded Euler (IEEE) scheme is developed. The SCSF scheme takes about 20–30 iterations for convergence, whereas the IEE scheme takes about 10 IE iterations and a few hundred of Euler equations iterations (over a very small computational domain) for convergence. The methods are applied to NACA 0012 and 64A010A airfoils over a wide range of Mach numbers. The results are in good agreement with the experimental data and other results that were obtained by using finite-difference and finite-volume methods with TSP, FP, and Euler equations.

Formulation

Full-Potential Equation

The dimensional equations of the two-dimensional, steady potential flow around an airfoil are given by

$$\Phi_{xx} + \Phi_{yy} = G \tag{1}$$

Received June 1, 1987; revision received Dec. 15, 1987.

*Professor, Department of Mechanical Engineering and Mechanics. Associate Fellow AIAA.

†Research Assistant, Department of Mechanical Engineering and Mechanics. Member AIAA.

$$G = (-1/\rho)(\rho_x \Phi_x + \rho_y \Phi_y) \tag{2}$$

$$\rho = [1 + (\gamma - 1/2)M_\infty^2(1 - \Phi_x^2 - \Phi_y^2)]^{(1/\gamma - 1)} \tag{3}$$

where Φ is the total velocity potential, ρ the density, M_∞ the freestream Mach number, γ the ratio of specific heats, and the subscripts x and y refer to the derivatives. It should be noted that G represents the total compressibility in the flow. The characteristic parameters are the freestream velocity U_∞, density ρ_∞, and the airfoil chord length ℓ.

The boundary conditions on the airfoil g, away from g, and at the trailing edge TE are given by

$$\nabla\Phi \cdot \hat{n} = 0 \qquad \text{on } g(x,y) = 0 \tag{4}$$

$$\nabla\Phi \to \bar{e}_\infty \qquad \text{away from } g \tag{5}$$

$$\Delta C_p|_{\text{TE}} = 0 \tag{6}$$

where $\hat{n} = \nabla g/|\nabla g|$, $\bar{e}_\infty$ is a unit vector parallel to $\bar{U}_\infty$, and ΔC_p is the pressure jump. The pressure coefficient is given by

$$c_p = \frac{2}{\gamma M_\infty^2}\left\{\left[1 + \frac{\gamma - 1}{2} M_\infty^2(1 - \Phi_x^2 - \Phi_y^2)\right]^{\frac{\gamma}{\gamma - 1}} - 1\right\} \tag{7}$$

The formal solution of Eq. (1) in terms of the velocity field $\nabla\Phi$ with explicit contribution of the shock surface S is obtained as

$$\begin{aligned}\nabla\Phi(x,y) = \bar{e}_\infty &+ \frac{1}{2\pi}\int_g q_g(s)\frac{(x-\varepsilon)\bar{i} + (y-\eta)\bar{j}}{(x-\varepsilon)^2 + (y-\eta)^2}\,ds \\ &+ \frac{1}{2\pi}\int_g \gamma_g(s)\frac{(y-\eta)\bar{i} - (x-\varepsilon)\bar{j}}{(x-\varepsilon)^2 + (y-\eta)^2}\,ds \\ &+ \frac{1}{2\pi}\int\int G(\varepsilon,\eta)\frac{(x-\varepsilon)\bar{i} + (y-\eta)\bar{j}}{(x-\varepsilon^2) + (y-\eta)^2}\,d\varepsilon\,d\eta \\ &+ \frac{1}{2\pi}\int_S q_S(s)\frac{(x-\varepsilon)\bar{i} + (y-\eta)\bar{j}}{(x-\varepsilon)^2 + (y-\eta)^2}\,ds\end{aligned} \tag{8}$$

where q_g and γ_g are the airfoil surface distribution of sources and vorticity, respectively, and q_S is the source strength of the shock surface. It should be noted that the last integral term on the right is used only for the shock-fitting part of the SCSF scheme. This term is included in the field integral term (third term on the right) and requires a very fine grid to obtain its effect. Since we use a relatively coarse grid, this term cannot fully have its effect in the shock-capturing part of the SCSF scheme. Therefore, in the shock-fitting part, we explicitly extract this term from the third integral and express it by the fourth integral to obtain its full accurate contribution.

For the shock fitting, we use the following equations of the Rankine-Hugoniot relations to determine the shock-segments strength q_S, orientation β, and the flow properties ρ_2, V_{2n}, and V_{2t} behind the shock.

$$q_S = -(V_{1n} - V_{2n}) = -\frac{2V_{1n}}{\gamma + 1}\left(1 - \frac{1}{M_{1n}^2}\right), \quad M_{1n} > 1 \tag{9}$$

$$\beta = \sin^{-1}\left[\frac{1.2\sin\beta\sin\theta}{\cos(\beta - \theta)} + \frac{1}{M_1^2}\right]^{\frac{1}{2}} \tag{10}$$

$$V_{2n} = \frac{(\gamma - 1)M_{1n}^2 + 2}{(\gamma + 1)M_{1n}^2} V_{1n} \tag{11}$$

$$V_{2t} = V_{1t} \tag{12}$$

$$\rho_2 = \frac{(\gamma + 1)M_{1n}^2}{(\gamma - 1)M_{1n}^2 + 2}\rho_1 \tag{13}$$

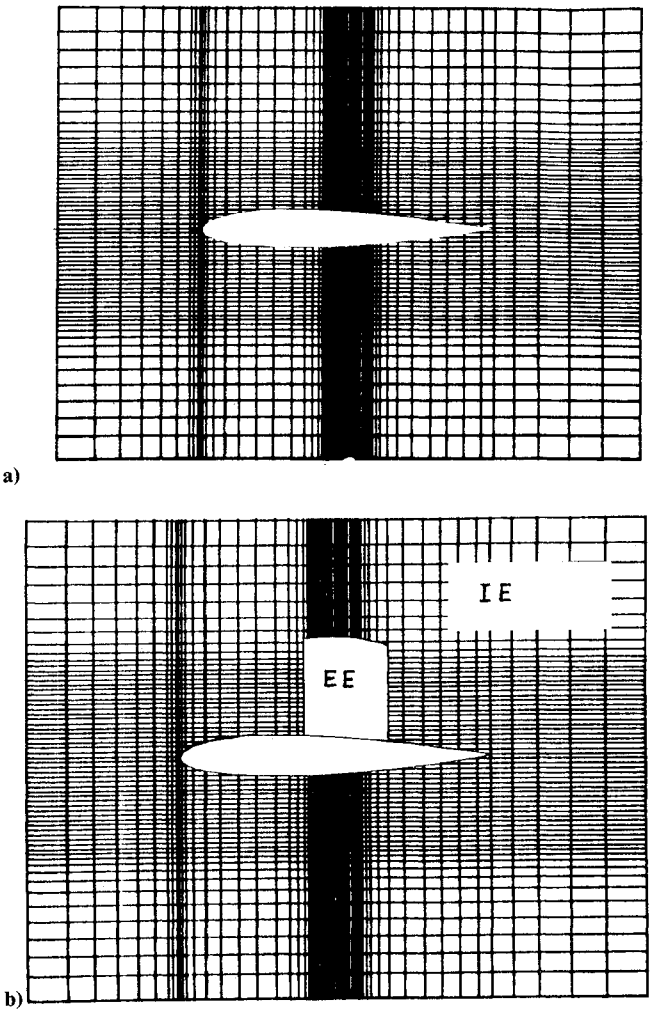

Fig. 1 Integral equation grid without and with an embedded-Euler domain.

where

$$M_1 = M_\infty|\nabla\Phi|_1 \Big/ \rho_1^{\frac{\gamma-1}{2}}, \qquad M_{1n} = M_\infty \nabla\Phi_1 \cdot \hat{n}_S \Big/ \rho_1^{\frac{\gamma-1}{2}} \tag{14}$$

In Eqs. (9–14), the subscripts 1 and 2 refer to the conditions ahead and behind the shock, respectively, while n and t refer to the normal and tangential directions to the shock surface S, respectively, and θ is the relative direction of the flow behind the shock to that ahead of the shock.

Euler Equations

For strong shocks, an embedded computational domain is constructed around the shock that has been found by using the shock-capturing part of the SCSF scheme. With the boundary and initial conditions found from the integral solution, the unsteady conservative form of the Euler equations are solved in this limited domain using a pseudotime marching. The dimensionless conservative form of these equations is given by

$$\frac{\partial\bar{q}}{\partial t} + \frac{\partial\bar{E}}{\partial x} + \frac{\partial\bar{F}}{\partial y} = 0 \tag{15}$$

where the flowfield vector $\bar{q}$ and the flux components $\bar{E}$ and $\bar{F}$ are given by

$$\bar{q} = [\rho, \rho u, \rho v, \rho e]^t \tag{16}$$

$$\bar{E} = [\rho u, \rho u^2 + p, \rho uv, \rho uh]^t \tag{17}$$

$$\bar{F} = [\rho v, \rho uv, \rho v^2 + p, \rho vh]' \tag{18}$$

The total energy and enthalpy per unit mass are given by

$$e = [p/(\gamma + 1)\rho] + (u^2 + v^2)/2, \qquad h = e + p/\rho \tag{19}$$

Since we are interested in the steady flow solution only, the energy equation [last elements in Eqs. (16–18)], which is a differential equation, is replaced by the algebraic steady form that states that the total enthalpy is constant. Hence, the energy equation is replaced by

$$p = (\rho/\gamma)[1/M_\infty^2 + (\gamma - 1)(1 - u^2 - v^2)/2] \tag{20}$$

Method of Solution

The airfoil surface is divided into small straight segments that are called surface or boundary panels. On each surface panel a piecewise linear distribution of two-dimensional sources and/or vorticity (q_g,γ_g) is defined in terms of local coordinates and their nodal values. A rectangler computational domain, which is divided into rectangular field elements, is constructed around the airfoil. The field elements adjacent to the airfoil surface are of trapezoidal shape. On each field element, a constant source distribution G is defined. The centroidal value of G represents the G value for the field element. Figure 1a shows a typical grid for transonic calculations using the SCSF scheme.

Shock Capturing-Shock Fitting Scheme

The basic differences between the incompressible integral equation solution and the transonic integral equation solution are the additional third and fourth integral terms of Eq. (8). In the shock-capturing part of the scheme, the fourth integral term is dropped, whereas in the shock-fitting part of the scheme this term is taken into account and is not considered in the third integral expression. This process is accomplished as follows. If a captured segment of a shock is inside a field element, the element is split into two subelements along the shock-segment boundary, where the fourth integral of Eq. (8) is used to determine the contribution of the shock segments. The third integral of Eq. (8) is used to determine the contributions of the two subelements.

The SCSF scheme is an iterative scheme due to the nonlinearity of the third and fourth integral terms. The iterative scheme is described below.

Setting $G = 0$ and $q_S = 0$, Eq. (8) is used through a standard panel computation to obtain q_g and/or γ_g. Initial values of G are calculated at the centroids of the field elements by using the linear compressibility relation $G = M_\infty^2 u_x$, where u_x is the x derivative of the x component of the velocity. It should be noted here that throughout the computational schemes, the centroidal value of G represents the G value for the field element. Equation (8) is then used to enforce the surface boundary condition and Kutta condition, Eqs. (4) and (6), respectively. The resulting set of equations are solved to find new q_g and/or γ_g. Next, the nonlinear compressibility G and density ρ are calculated by using Eqs. (2) and (3). A type-difference expression is used to calculate ρ_x and ρ_y, depending on the type of the centroidal point-subsonic or supersonic. Once the G values are obtained, the surface boundary condition and the Kutta condition are satisfied again. The iterative procedure is continued until the shock location is fixed. This is the shock-capturing part of the scheme. It is a two-dimensional application of the shock-capturing scheme by Kandil and Yates.[12]

Shock panels are then introduced at the shock location, the fourth integral term of Eq. (8) is now taken into account, Eqs. (9) and (10) are used to calculate q_s and β, and Eqs. (10–13) are used to cross the shock panel. The iterative procedure is continued as before with the exception of dealing with the shock panels as explained. Shock location and shape are allowed to vary during the iterative procedure. Convergence is achieved once the surface pressure converges. This is the shock-fitting part of the scheme.

Integral Equation-Embedded Euler Scheme

In this scheme the shock-capturing part of the SCSF scheme is used to locate the shock. Once the shock is captured, a fine grid is constructed within a small computational domain around the shock where a finite-volume Euler scheme is used. Figure 1b shows a typical grid with the embedded Euler domain. The basic finite-volume equation is obtained by integrating Eq. (15) over x and y to obtain

$$\int\int \frac{\partial q}{\partial t}\, dA + \S(E\, dy + F\, dx) = 0 \tag{21}$$

Equation (21) is then applied to each cell of the embedded grid of the Euler domain. The resulting difference equation is

$$\left(\frac{\partial q}{\partial t}\right)_{ij} \Delta A_{ij} + \sum_{r=1}^{4} (E\Delta y_r + F\Delta x_r) = 0 \tag{22}$$

where ΔA is the cell area, r refers to the cell-side number, and the integer subscripts i and j refer to the centroidal values. The Euler solver is a central-difference finite-volume method that used four-stage Runge-Kutta time stepping with explicit second- and fourth-order dissipation terms.[17]

The boundary and initial conditions for the Euler domain are obtained from the integral equation solution. They are interpolated on the Euler domain grid. The Euler solver is then used to capture the shock and calculate the flowfield vector $\bar{q}$. Fixing the $\bar{q}$ values of the Euler domain, the IE calculation is used to update the boundary conditions for the Euler domain. The iterative procedure is repeated until convergence is achieved.

Since Euler equations do not assume isentropic flow, and hence entropy increase and vorticity production develop at the shock, one has to extract the vorticity from the flow at the downstream boundary of the Euler domain. This is accomplished as follows. During the solution of Euler equations in its domain, the downstream boundary condition is updated. When the IE solution is performed, an overlap region between

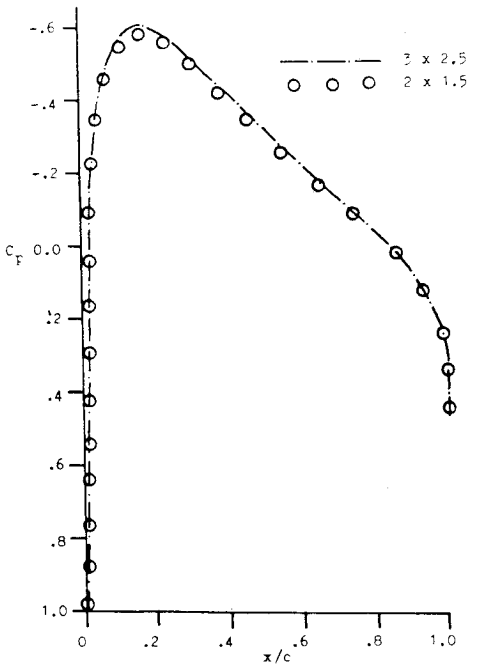

Fig. 2 Effect of the computational domain size, surface vortex panels, NACA 0012, $M_\infty = 0.72$, $\alpha = 0^0$.

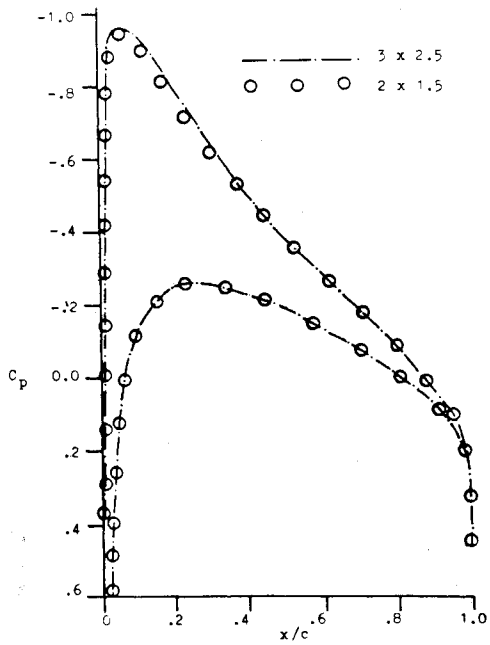

Fig. 3 Effect of the computational domain size, surface vortex panels, NACA 0012, $M_\infty = 0.63$, $\alpha = 2^0$.

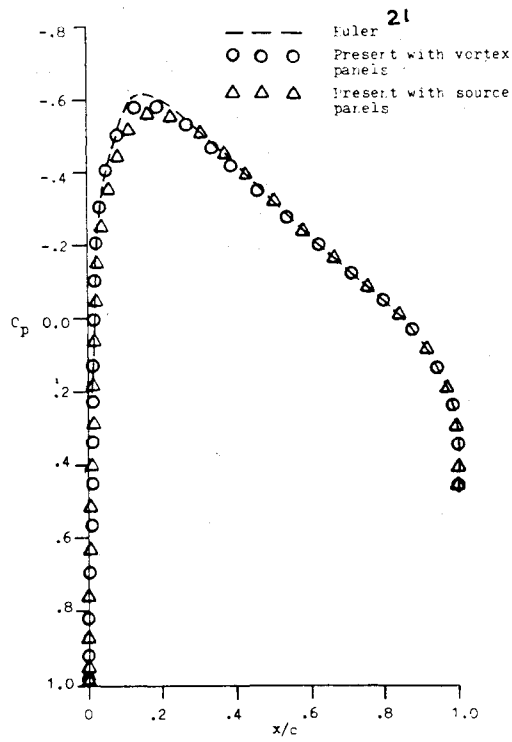

Fig. 4 Comparisons of IE solution with surface vortex panels and surface source panels with Euler solution, NACA 0012, $M_\infty = 0.72$, $\alpha = 0^0$.

Euler equation domain and the IE domain is created, where the IE solution is also used.

Numerical Examples

Shock-Free Flows

The first step to validate the computer program is to check the sensitivity of the IE solution to the size of the computational domain. Figure 2 shows the solutions for the NACA 0012 airfoil at $M_\infty = 0.72$ and $\alpha = 0^0$ using vortex panels only on the airfoil surface. We used a total of 140 vortex panels on

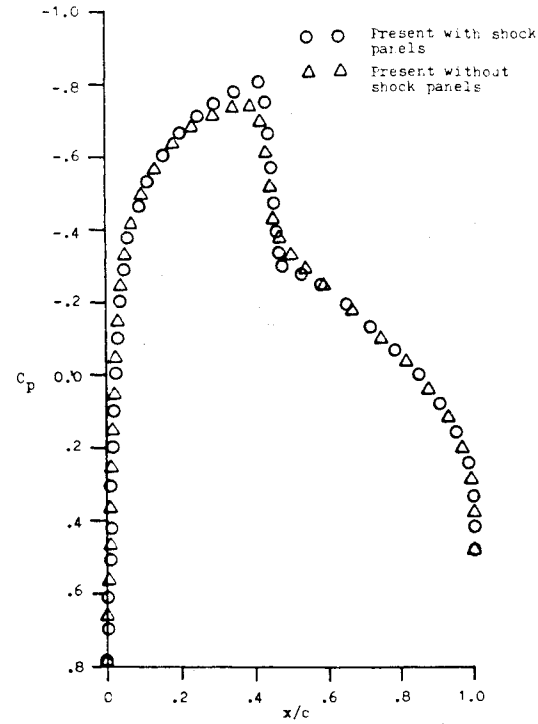

Fig. 5 Shock-capturing vs SCSF scheme, NACA 0012, $M_\infty = 0.8$, $\alpha = 0^0$.

the airfoil surface and 64 × 60 field elements in a computational region around the airfoil. The solutions show the surface pressure using two sizes of the computational domains: 2 × 1.5 and 3 × 2.5 (a unit length represents the chord length). In Fig. 3 we repeat the same test for a lifting case of the same airfoil at $M_\infty = 0.63$ and $\alpha = 0^0$. The results of these two cases show that a computational domain of 2 × 1.5 gives as accurate solutions as those of the 3 × 2.5 computational domain. A computational region of 3 × 2.5 with 80 × 80 field elements was also used, and the results did not show appreciable changes from those of the 2 × 1.5 and 64 × 60 case.

The second numerical test is aimed at comparing the results of the IE solution using vortex panels only and source panels only with the solution of Euler equations. Figure 4 shows the results of this test for the NACA 0012 airfoil at $M_2 = 0.7$ and $\alpha = 0^0$. The computational domain is 2 × 1.5, and the same numbers of surface panels and field elements as those of Fig. 2 have been used. It is clear that the IE solution with surface vortex panels is superior to that of the source panels. A typical case of shock-free flows requires about six iterations for convergence of the surface pressure.

As a result of these numerical tests, it is decided to use a computational domain of 2 × 1.5 for the other computations with the exception of the cases with strong shocks, where the computational domain was as large as 3 × 4.

Since the third integral term of Eq. (8) is computationally expensive, its computation with constant G distribution has been restricted to the near-field computation. For the far-field computation, this term is replaced by the equivalent lumped source term at its centroid. With sufficient accuracy, it has been computationally determined that the near-field distance from the centroid is ≤ 0.5.

Transonic Flows

First, we present a numerical test case to show the effect of introducing the shock panels and their fitting as explained earlier. Figure 5 shows a comparison between the shock-capturing results and the SCSF scheme results for the NACA 0012 airfoil at $M_\infty = 0.8$ and $\alpha = 0^0$. It is clear that the SCSF scheme sharpens the shock, as expected, with this relatively coarse grid.

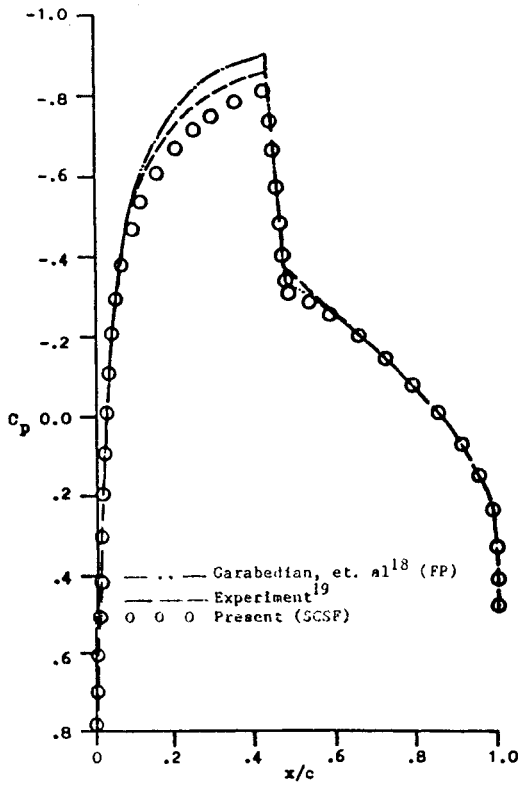

Fig. 6 Integral equation solution with SCSF scheme, NACA 0012, $M_\infty = 0.8$, $\alpha = 0^0$.

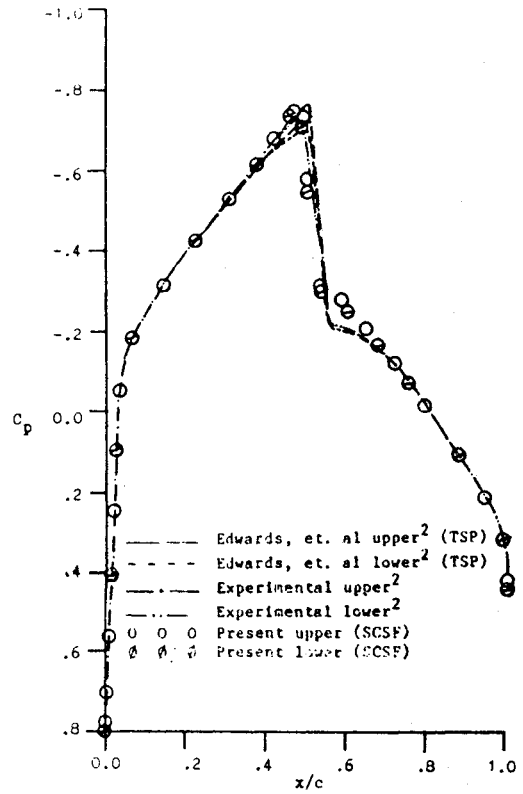

Fig. 8 Integral equation solution with SCSF scheme, NACA 64A010A, $M_\infty = 0.796$, $\alpha = 0^0$.

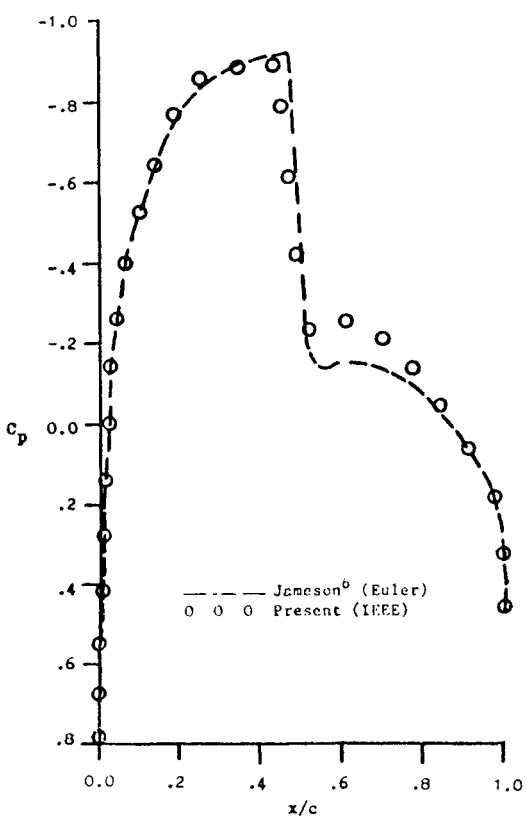

Fig. 7 Integral equation with embedded-Euler domain solution, NACA 0012, $M_\infty = 0.8$, $\alpha = 0^0$.

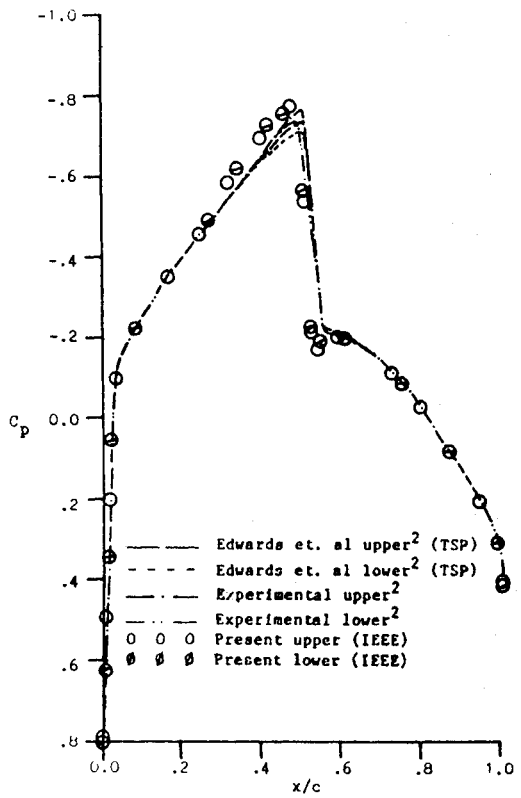

Fig. 9 Integral equation with embedded-Euler domain solution, NACA 64A010A, $M_\infty = 0.796$, $\alpha = 0^0$.

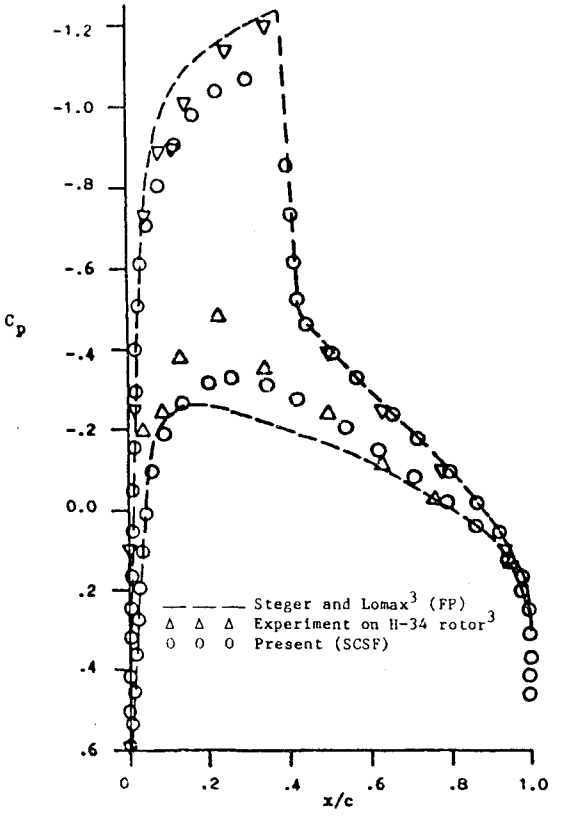

Fig. 10 Integral equation solution with SCSF scheme, NACA 0012, $M_\infty = 0.75$, $\alpha = 2^0$.

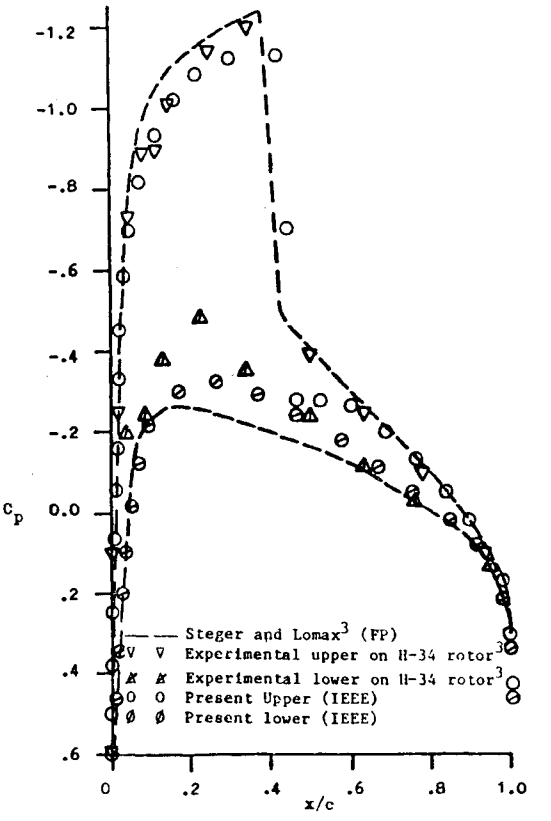

Fig. 11 Integral equation with embedded-Euler domain solution, NACA 0012, $M_\infty = 0.75$, $\alpha = 2^0$.

Next, we compare the SCSF scheme with the experimental data and other computational results. Figure 6 shows the results of the SCSF scheme for NACA 0012, $M_\infty = 0.8$ and $\alpha = 0^0$, along with comparisons with the computational results of Garabedian et al.,[18] and the experimental data taken from Ref. 19. The SCSF results slightly underpredict the experimental data in the supersonic region and at the shock. The SCSF scheme took 12 iteration cycles of shock capturing (SC) and 13 cycles of shock fitting (SF) to achieve convergence.

Figure 7 shows the results of the IEEE scheme for the same case along with a comparison with the computational results of Jameson,[5] who also used the finite-volume Euler scheme with four-stage Runge-Kutta time stepping. In the present IEEE scheme, the embedded Euler domain has a size of 0.5×0.6 around the shock region with a grid of 25×30. This case took 10 iteration cycles of SC, 250 times cycles of Euler iterations to achieve a residual error of 10^{-3}, and 5 IE cycles to update the Euler domain boundary conditions. The IEEE results predict stronger shock as compared with the experimental data of Fig. 6, typical of Euler results. Also, the IEEE scheme overpredicts the pressure behind the shock as compared to Jameson's Euler results. This may be attributed to the short overlap between the Euler domain and the IE domain.

Figures 8 and 9 show the results of the SCSF and IEEE schemes for NACA 64A010A, $M_\infty = 0.796$ and $\alpha = 0^0$ along with comparisons with the computational results of Edwards et al.,[2] who used the TSP equation, and the experimental data taken from Ref. 2. With the SCSF scheme, the numbers of SC and SF iteration cycles to achieve convergence are the same as those of the case presented in Fig. 6. With the IEEE scheme, the embedded Euler domain has a size of 0.7×0.6 with a grid size of 35×30. This case, Fig. 9, took 10 iteration cycles of SC, 130 time cycles of Euler iterations to achieve a residual error of 10^{-3}, and 3 IE cycles to update the Euler domain boundary conditions. Again, it is observed that the SCSF scheme predicts a slightly weaker shock than the experimental data, whereas the IEEE scheme predicts a slightly stronger shock than the experimental data.

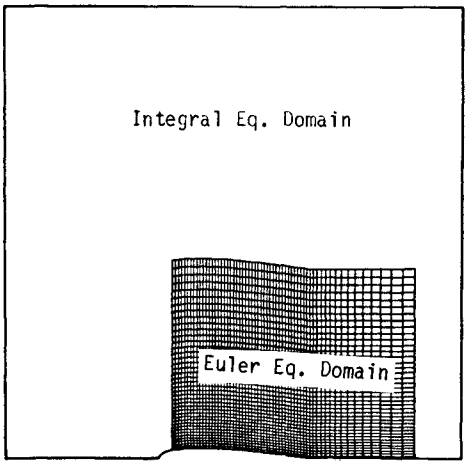

Fig. 12 Embedded Euler domain and grid for strong shocks.

Figures 10 and 11 show the results of SCSF and IEEE schemes for the lifting case of NACA 0012, $M_\infty = 0.75$ and $\alpha = 2^0$, along with the computational results of Steger and Lomax,[3] and the experimental data taken from the same reference. The size of the grids and the number of iteration cycles used to achieve convergence are the same as those of the cases given in Figs. 6 and 7. In the supersonic region, both the SCSF and IEEE schemes slightly underpredict the surface pressure of the experimental data.

For stronger shocks than those considered above, the IE computational domain is extended in the longitudinal and lateral directions, and so is the embedded Euler computational domain. The Euler domain is extended beyond the trailing edge to allow for the vorticity to be shed downstream, where the overlapping region with the IE equation exists. Figure 12 shows a typical computational domain with details of the embedded Euler domain.

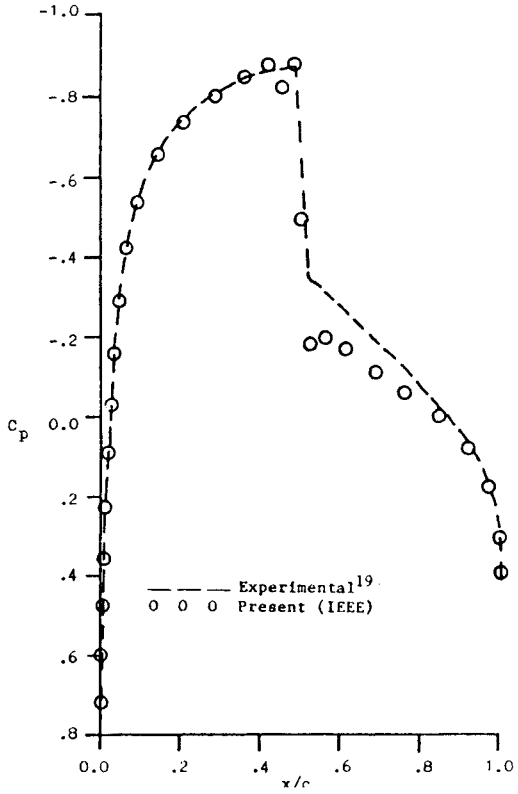

Fig. 13 Integral equation with embedded-Euler domain solution, NACA 0012, $M_\infty = 0.812$, $\alpha = 0^0$.

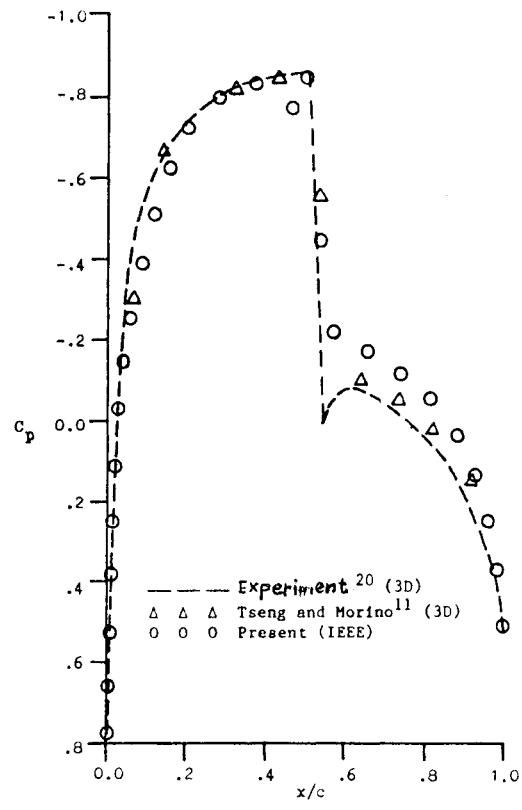

Fig. 14 Integral equation with embedded-Euler domain solution, NACA 0012, $M_\infty = 0.82$, $\alpha = 0^0$.

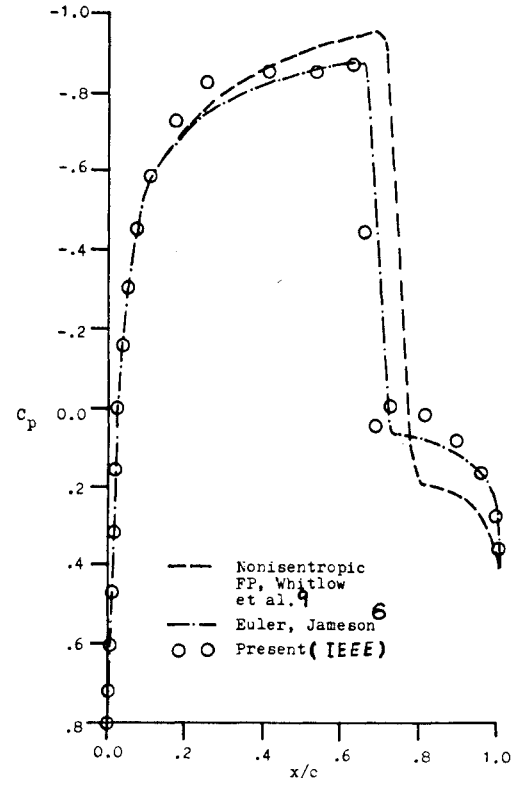

Fig. 15 Integral equation with embedded-Euler domain solution, NACA 0012, $M_\infty = 0.84$, $\alpha = 0^0$.

Next, we show the results of the IEEE scheme for cases of strong shocks.

Figure 13 shows the results of the IEEE for NACA 0012, $M_\infty = 0.812$ and $\alpha = 0^0$, along with the experimental data of Ref. 18. In Fig. 14 the results of the IEEE for NACA 0012, $M_\infty = 0.82$ and $\alpha = 0^0$, are shown along with the three-dimensional solution at the wing root chord of Tseng and Morino,[11] who use the IE for the TSP, and the experimental results of Ref. 20. The size of the embedded Euler domain for these cases is 0.8×0.8, and its grid size is 40×40.

Figure 15 shows the results of the IEEE for NACA 0012, $M_\infty = 0.84$ and $\alpha = 0^0$, along with comparisons with the nonisentropic FP solution of Whitlow et al.,[9] and the Euler equations solution Jameson.[6] The size of the embedded Euler domain for this case is 1.5×1.0, and its grid size is 60×40. This case took 10 IE iterations 300 time cycles of Euler iterations, and 3 IE cycles to update the Euler domain boundary conditions.

On the CYBER-185 computer at the NASA Langley Research Center, for 65×60 field panels an IE iteration cycle takes about 200 CPU seconds. For 25×30 cells an Euler cycle takes about 2 CPU seconds on the same computer.

Concluding Remarks

Two computational methods, which are based on the integral equation solution of the full-potential equation, have been presented. In the first method, a shock capturing-shock fitting scheme has been developed, while in the second method, an integral equation-embedded Euler scheme has been developed. The SCSF scheme consists of two parts: a shock-capturing part where the shock is captured through an iterative procedure using the integral solution, and a shock-fitting part where shock panels are fitted by using the Rankine-Hugoniot relations. The IEEE scheme couples the shock-capturing part of the SCSF scheme with an embedded region where Euler equations are integrated in pseudotime marching. The Euler solver

is a central-difference finite-volume scheme with four-stage Runge-Kutta time stepping.

The two schemes are applied to several transonic airfoil flows; the results have been compared with numerous computational results and with experimental data, and they are in good agreement. The two schemes are nevertheless efficient in terms of the number of iterations, as compared to the other existing schemes that use finite-difference or finite-volume methods throughout large computational domains with fine grids. If the influence coefficients of the field elements are stored in the core memory of the computer, the computational time of the IE cycle can substantially be reduced, since the field-elements calculations represent about 80% of the computational time per iteration cycle. The SCSF scheme is restricted to flows with weak shocks, whereas the IEEE scheme can handle strong shocks.

Currently, pseudotime integration and time-accurate integration of the integral equation solution are tested with and without embedded Euler domains. The idea here is to enforce hyperbolicity in the integral equation through the time-marching procedure.

Acknowledgment

This research work has been supported by NASA Langley Research Center under Grant NAG-1-648.

References

[1]Murman, E. M. and Cole, J. D., "Calculation of Plane Steady Transonic Flows," *AIAA Journal*, Vol. 9, Jan. 1971, pp. 114–121.

[2]Edwards, J. W., Bland, S. R., and Seidel, D. A., "Experience with Transonic Unsteady Aerodynamic Calculations," NASA TM-86278, 1984.

[3]Steger, J. L. and Lomax, H., "Transonic Flow about Two-Dimensional Airfoils by Relaxation Procedures," *AIAA Journal*, Vol. 10, Jan. 1972, pp. 49–54.

[4]Garabedian, P. R. and Korn, D., "Analysis of Transonic Airfoils," *Communication of Pure and Applied Mathematics,* Vol. 24, No. 6, Nov. 1971, pp. 841–851.

[5]Jameson, A., "Iterative Solution of Transonic Flows Over Airfoils and Wings," *Communication of Pure and Applied Mathematics,* Vol. 27, May 1974, pp. 283–309.

[6]Jameson, A., "Transonic Airfoil Calculations Using the Euler Equations," *Numerical Methods in Aeronautical Fluid Dynamics*, edited by P. L. Roe, Academic, New York, 1982, pp. 289–309.

[7]Hafez, M. and Lovell, D., "Entropy and Vorticity Corrections for Transonic Flows," AIAA Paper 83-1926, 1983.

[8]Fuglsang, D. F. and Williams, M. H., "Non-Isentropic Unsteady Transonic Small Disturbance Theory," AIAA Paper 85-0600, 1985.

[9]Whitlow, W., Jr., Hafez, M. M., and Osher, S. J., "An Entropy Correction Method for Unsteady Full Potential Flows with Strong Shocks," NASA TM-87769, 1986.

[10]Piers, W. J. and Sloof, J. W., "Calculations of Transonic Flow by Means of a Shock-Capturing Field Panel Method," AIAA Paper 79-1459, 1979.

[11]Tseng, K. and Morino, L., "Nonlinear Green's Function Methods for Unsteady Transonic Flows," *Transonic Aerodynamics*, edited by D. Nixon, AIAA, New York, 1982, pp. 565–603.

[12]Kandil, O. A. and Yates, E. C., Jr., "Computation of Transonic Vortex Flows past Delta Wings—Integral Equation Approach," *AIAA Journal*, Vol. 24, Nov. 1986, pp. 1729–1736.

[13]Oskam, B., "Transonic Panel Method for the Full Potential Education Applied to Multicomponent Airfoils," *AIAA Journal*, Vol. 23, Sept. 1985, pp. 1327–1334.

[14]Erickson, L. L. and Strande, S. M., "A Theoretical Basis for Extending Surface—Paneling Methods to Transonic Flow," *AIAA Journal*, Vol. 23, Dec. 1985, pp. 1860–1867.

[15]Sinclair, P. M., "An Exact Integral (Field Panel) Method for the Calculation of Two-Dimensional Transonic Potential Flow Around Complex Configurations," *Aeronautical Journal*, Vol. 90, No. 896, June–July 1986, pp. 227–236.

[16]Kandil, O. A. and Hu, H., "Integral Equation Solution for Transonic and Subsonic Aerodynamics," Third GAMM Seminar on Panel Methods in Mechanics, Kiel, FRG, Jan. 1987.

[17]Kandil, O. A. and Chuang, A., "Influence of Numerical Dissipation in Computing Supersonic Vortex-Dominated Flows," *AIAA Journal*, Vol. 25, Nov. 1987, pp. 1426–1434.

[18]Bauer, F., Garabedian, P., and Koru, D., "Supercritical Wing Sections," *Lecture Notes in Economics and Mathematical Systems*, Vol. 66, Springer-Verlag, New York, 1972.

[19]Hall, M. G., *Transonic Flows*, IMA, Controller, HMSO, London, 1975.

[20]Lee, K. D., Dickson, L. J., Chen, A. W., and Rubbert, P. E., "An Improved Matching Method for Transonic Computations," AIAA Paper 78-1116, 1978.

[21]Sells, C. L., "Plane Subcritical Flow Past a Lifting Airfoil," *Proceedings of the Royal Society of London*, Series A, Vol. 308, No. 1494, Jan. 1969, pp. 377–401.